PRAMANA
— journal of
physics

Vol. 65, No. 1
July 2005
pp. 95–105

The analytical investigation of the super-Gaussian pump source on the thermal, stress and thermo-optics properties of double-clad Yb:glass fiber lasers

H NADGARAN and P ELAHI
Department of Physics, College of Science, Shiraz University, Shiraz 71454, Iran
E-mail: nadgaran@susc.ac.ir; phy1pe@sccc.susc.ac.ir; Phy1pe@yahoo.com

MS received 23 June 2004; revised 22 December 2004; accepted 16 February 2005

Abstract. Fiber lasers have attracted considerable attention when their power can realistically be scaled to kilowatt level and beyond. In this paper, we assumed that the fiber core and first clad are exposed to a pump source with a super-Gaussian profile of order four. The effects of this non-uniform heat deposition on thermal, stress and thermo-optics properties such as temperature-dependent change of refractive index and thermally induced stress have been comprehensively studied and their equations analytically derived.

Keywords. Diode-pumped fiber lasers; thermal effects in fiber lasers; super-Gaussian beam profile.

PACS Nos 42.55.Wd; 42.55.Xi; 42.25.Lc

1. Introduction

Fiber lasers, an extreme case of end-pump lasers, have been the subject of considerable attention recently [1–3]. The low-loss rare-earth-doped fiber has led to the construction of low threshold, efficient operation and single-mode fiber lasers [4–8]. In power scaling studies of high-power fiber lasers, the role of thermally induced stress and other thermo-optics effects acquire much attention because standard fiber designs will eventually lead to high core temperature when dealing with high power regimes [9]. Therefore, the usual practice of neglecting thermal effects can no longer be justified. Recent modeling of thermal effects of Yb:glass fiber lasers [10] has revealed that a careful management of these effects can remarkably reduce the handling of these lasers when performing scaling up efforts. Those works, however, assume a top-hat shape deposition of heat power density into the fiber. This work is an extension of such works in which a non-uniform multi-mode super-Gaussian profile is assumed for the laser pump. The multi-mode assumption of the pump source is essential, since when the source power increased, this matter is inevitable.

Here too, double-clad fibers in which a core of Yb-doped ions surrounded by a lower index cladding which is in turn covered by a second cladding of even lower index are studied. The core host material and cladding of the fiber are assumed to have the same thermal and mechanical properties. The analytical solutions of heat distribution equation for such fibers in the two distinct regions of the fiber, namely the core and cladding regions are first presented in §2. This section continues with appropriate application of boundary conditions. Section 3 shows the equations governing the thermally induced stress and the change of index of refraction due to stress. The equation for temperature-dependent change of the refractive index in the fiber has been discussed in §4. Section 5 presents a comprehensive analysis of Yb:glass fiber laser, based on derivations from other sections and a summary of the results. The summary and recommendations for future works appear in §6.

2. Radial temperature distribution of the fiber

Investigation of heat distributions in the fiber is essential for calculating the thermo-optics properties of fiber lasers. We begin by finding the radial heat distribution of a fiber whose core and cladding radii are a and b respectively. The radial coordinate is r and the azimuthal angle is φ. The steady state heat equation for an isotropic medium can be written as [11]

$$\nabla^2 T(r,z) = -\frac{S(r)}{k}, \tag{1}$$

where k and $S(r)$ are the medium thermal conductivity and heat power density of the source respectively. For finding the temperature distribution, $T(r,z)$, the following assumptions have been made:

(1) The physical and mechanical properties of the two distinct fiber regions, namely, the core and the outer region of the core over a given temperature range remain constant, i.e. linear solutions of eq. (1) are assumed.
(2) The core and cladding regions are assumed to be circular and concentric.
(3) The modeling and analysis are performed time independently, because it is supposed that the fiber core is continuously exposed to pump radiation.
(4) Because optical fibers are high aspect ratio devices, i.e., their length L is much greater than the diameter, the z derivative term of eq. (1) can be neglected.

Suppose the fiber is irradiated by a super-Gaussian beam profile of order four as:

$$S(r) = Q \exp\left(\frac{-r^4}{\omega_0^4}\right), \tag{2}$$

where ω_0 is the spot size and Q is the heat power density.

The steady state heat equation in the core and cladding regions can then be written as

$$\frac{1}{r}\frac{\partial}{\partial r}\left(r\frac{\partial}{\partial r}T_1(r)\right) = -\beta \exp\left(\frac{-r^4}{\omega_0^4}\right), \quad 0 \le r \le a \tag{3}$$

for the core region and

$$\frac{1}{r}\frac{\partial}{\partial r}\left(r\frac{\partial}{\partial r}T_2(r)\right)=0, \quad a\le r\le b \tag{4}$$

for the cladding region.

Here

$$\beta=\frac{Q}{k}. \tag{5}$$

It is seen that $S(r)$ abruptly goes to zero in the cladding region since heat is generated mainly in the rare-earth-doped fiber core due to quantum defect between the pump and the laser photons [11]. In other words, the doped ions are responsible for the heat generation within the core, whereas they are absent in the cladding region.

The solutions of eqs (3) and (4) are

$$T_1(r)=-\frac{Q}{4k}\,{}_2F_2\left(\frac{1}{2},\frac{1}{2},\frac{3}{2},\frac{3}{2};-\frac{r^4}{\omega_0^4}\right)r^2+A\ln(r)+T_0, \quad 0\le r\le a \tag{6}$$

for the core region where T_0 is the temperature at the center of the fiber, and

$$T_2(r)=B+C\ln\left(\frac{r}{a}\right), \quad a\le r\le b \tag{7}$$

for the cladding region. A, B and C are constants and ${}_kF_l(a_1,a_2,\ldots,a_k,b_1,b_2,\ldots,b_l;x)$ is the hypergeometric function defined by [12]

$${}_kF_l\left(a_1,a_2,\ldots,a_k,b_1,b_2,\ldots,b_l;x\right)=\sum_{n=0}^{\infty}\frac{(a_1)_n(a_2)_n\cdots(a_k)_n}{(b_1)_n(b_2)_n\cdots(b_l)_n}\,\frac{x^n}{n!}, \tag{8}$$

where use has been made of Pochhammer symbol, $(a_k)_n$ and $(b_l)_n$ defined as

$$\begin{aligned}&(a_k)_n=a_k(a_k+1)(a_k+2)\cdots(a_k+n-1)\\&a_0=1.\end{aligned} \tag{9}$$

2.1 *Boundary conditions*

The following boundary conditions have been used to obtain the constants A, B and C. The finiteness of $T_1(r)$ at the center of the fiber immediately gives $A=0$. Therefore,

$$T_1(r)=-\frac{Q}{4k}\,{}_2F_2\left(\frac{1}{2},\frac{1}{2},\frac{3}{2},\frac{3}{2};-\frac{r^4}{\omega_0^4}\right)r^2+T_0. \tag{10}$$

Moreover, as $T_1|_{r=a}=T_2\,|_{r=a}$ we have

$$B = -\frac{Q}{4k}\,{}_2F_2\left(\frac{1}{2},\frac{1}{2},\frac{3}{2},\frac{3}{2};-\frac{a^4}{\omega_0^4}\right)a^2 + T_0, \tag{11}$$

and the continuity of the radial derivatives at the boundary, i.e.,

$$\left.\frac{\mathrm{d}T_1}{\mathrm{d}r}\right|_{r=a} = \left.\frac{\mathrm{d}T_2}{\mathrm{d}r}\right|_{r=a} \tag{12}$$

gives

$$C = -\frac{Q}{4k}a^2\Bigg[2\,{}_2F_2\left(\frac{1}{2},\frac{1}{2},\frac{3}{2},\frac{3}{2};-\frac{a^4}{\omega_0^4}\right) -\frac{4}{9}\left(\frac{a}{\omega_0}\right)^4\,{}_2F_2\left(\frac{3}{2},\frac{3}{2},\frac{5}{2},\frac{5}{2};-\frac{a^4}{\omega_0^4}\right)\Bigg]. \tag{13}$$

Moreover, from the following conditions

$$\left.\frac{\mathrm{d}T_2}{\mathrm{d}r}\right|_{r=b} = \frac{h}{k}\left(T_\mathrm{c} - T\,|_{r=b}\right) \tag{14}$$

where T_c is the ambient temperature, we then obtain

$$C\left(\frac{k}{bh} + \ln\left(\frac{b}{a}\right)\right) = T_\mathrm{c}B. \tag{15}$$

Equations (11), (13) and (15) will end up with explicit B constants as

$$B = T_\mathrm{c} - \frac{Q}{4k}a^2\Bigg[2\,{}_2F_2\left(\frac{1}{2},\frac{1}{2},\frac{3}{2},\frac{3}{2};-\frac{a^4}{\omega_0^4}\right) -\frac{4}{9}\left(\frac{a}{\omega_0}\right)^4\,{}_2F_2\left(\frac{3}{2},\frac{3}{2},\frac{5}{2},\frac{5}{2};-\frac{a^4}{\omega_0^4}\right)\Bigg]\left[\frac{k}{bh} + \ln\left(\frac{b}{a}\right)\right] \tag{16}$$

and

$$T_0 = +\frac{Q}{9k}a^2\left[\frac{k}{bh} + \ln\left(\frac{b}{a}\right)\right]\left(\frac{a}{\omega_0}\right)^2\,{}_2F_2\left(\frac{3}{2},\frac{3}{2},\frac{5}{2},\frac{5}{2};-\frac{a^4}{\omega_0^4}\right) +\frac{Q}{4k}a^2\,{}_2F_2\left(\frac{1}{2},\frac{1}{2},\frac{3}{2},\frac{3}{2};-\frac{a^4}{\omega_0^4}\right)\left[1 - 2\left(\frac{k}{bh} + \ln\left(\frac{b}{a}\right)\right)\right] + T_\mathrm{c}. \tag{17}$$

Having found all constants and T_0, we summarize the temperature distribution of the core and cladding as

$$T_1(r) = -\frac{Q}{4k}{}_2F_2\left(\frac{1}{2},\frac{1}{2},\frac{3}{2},\frac{3}{2};-\frac{r^4}{\omega_0^4}\right)r^2 - \frac{Q}{9k}a^2\left[\frac{k}{bh} + \ln\left(\frac{b}{a}\right)\right]\left(\frac{a}{\omega_0}\right)^2 +{}_2F_2\left(\frac{3}{2},\frac{3}{2},\frac{5}{2},\frac{5}{2};-\frac{a^4}{\omega_0^4}\right)\frac{Q}{4k}a^2\,{}_2F_2\left(\frac{1}{2},\frac{1}{2},\frac{3}{2},\frac{3}{2};-\frac{a^4}{\omega_0^4}\right) \times\left[1 + 2\left(\frac{k}{bh} + \ln\left(\frac{b}{a}\right)\right)\right] \tag{18}$$

for the core region, and

$$T_2(r) = T_c - \frac{Q}{4k}a^2\left[2\ {}_2F_2\left(\frac{1}{2},\frac{1}{2},\frac{3}{2},\frac{3}{2};-\frac{a^4}{\omega_0^4}\right)\right.$$
$$\left.-\frac{4}{9}\left(\frac{a}{\omega_0}\right)^4\ {}_2F_2\left(\frac{3}{2},\frac{3}{2},\frac{5}{2},\frac{5}{2};-\frac{a^4}{\omega_0^4}\right)\right]$$
$$\times\left[\frac{k}{bh}+\ln\left(\frac{b}{a}\right)\right]-\frac{Q}{4k}a^2\left[2\ {}_2F_2\left(\frac{1}{2},\frac{1}{2},\frac{3}{2},\frac{3}{2};-\frac{a^4}{\omega_0^4}\right)\right.$$
$$\left.-\frac{4}{9}\left(\frac{a}{\omega_0}\right)^4\ {}_2F_2\left(\frac{3}{2},\frac{3}{2},\frac{5}{2},\frac{5}{2};-\frac{a^4}{\omega_0^4}\right)\right]\ln\left(\frac{r}{a}\right) \tag{19}$$

for the cladding region.

Previous workers [10], who used a top-hat heat deposition to fiber, assumed the following differential equations in the core and cladding regions:

$$\frac{1}{r}\frac{\partial}{\partial r}\left(r\frac{\partial}{\partial r}T_1(r)\right) = -\frac{Q_0}{k}, \quad 0 \le r \le a,$$
$$\frac{1}{r}\frac{\partial}{\partial r}\left(r\frac{\partial}{\partial r}T_2(r)\right) = 0, \quad a \le r \le b, \tag{20}$$

A constant heat power density (Q_0) deposition to the core was essential for this type of analysis. The solution to eqs (20) according to the same boundary conditions discussed in §2.1 of our work are as follows:

$$T_1(r) = T_0 - \frac{Q_0 r^2}{4k}, \quad 0 \le r \le a,$$
$$T_2(r) = T_0 - \frac{Q_0 a^2}{4k} - \frac{Q_0 a^2}{4k}\ln\left(\frac{r}{a}\right), \quad a \le r \le b. \tag{21}$$

On Comparing, one can see the main difference between the temperature distribution within the core for the two cases of super-Gaussian and top-hat pump source. In the latter case, $T_1(r)$ is varying with r^2 whereas in the super-Gaussian case, it is a complex function including hypergeometric and logarithmic variations.

3. Thermally-induced stress under super-Gaussian pump source

Thermally-induced stress components resulting from the fiber heat can be written as follows [10]:

$$\sigma_r(r) = \frac{\alpha_T E}{(1-\nu)}\left[F - R(r)\right],$$
$$\sigma_\varphi(r) = \frac{\alpha_T E}{(1-\nu)}\left[F + R(r) - T(r)\right],$$
$$\sigma_z(r) = \frac{\alpha_T E}{(1-\nu)}\left[2F - T(r)\right], \tag{22}$$

where E, ν and α_{T} are Young's modulus, Poisson's ratio and thermal expansion coefficient of the core respectively. F and $R(r)$ are defined as [10]

$$F = \frac{1}{b^2}\int_0^b T(r) r \,\mathrm{d}r, \tag{23}$$

$$R(r) = \frac{1}{r^2}\int_0^r T(r) r \,\mathrm{d}r. \tag{24}$$

Substituting eqs (7) and (10) into eqs (23) and (24), F and $R(r)$ can be explicitly derived in the term of B, C and T_0 as:

$$F = \frac{1}{b^2}\left[-\frac{Qa^4}{16k}\,{}_3F_3\left(\frac{1}{2},\frac{1}{2},1,\frac{3}{2},\frac{3}{2},2;\frac{-a^4}{\omega_0^4}\right)+\frac{a^2}{2}T_0\right] + \frac{1}{2a^2}\left[Bb^2\ln\left(\frac{b}{a}\right)+\left(a^2-b^2\right)\left(\frac{B}{2}-C\right)\right], \tag{25}$$

$$R_1(r) = \frac{1}{r^2}\left[-\frac{Qr^4}{16k}{}_3F_3\left(\frac{1}{2},\frac{1}{2},1,\frac{3}{2},\frac{3}{2},2;\frac{-r^4}{\omega_0^4}\right)+\frac{r^2}{2}T_0\right], \quad 0 \le r \le a, \tag{26}$$

$$R_2(r) = \frac{1}{r^2}\left[-\frac{Qa^4}{16k}{}_3F_3\left(\frac{1}{2},\frac{1}{2},1,\frac{3}{2},\frac{3}{2},2;\frac{-a^4}{\omega_0^4}\right)+\frac{a^2}{2}T_0\right] + \frac{1}{2r^2}\left[Br^2\ln\left(\frac{r}{a}\right)+\left(a^2-r^2\right)\left(\frac{B}{2}-C\right)\right], \quad a \le r \le b, \tag{27}$$

where B, C, and T_0 are constants as obtained in eqs (13), (16), and (17). Having derived expressions for F and $R(r)$, radial, tangential and z stress can be calculated using eq. (22).

Finally, the change of refractive index induced by thermal stress can be calculated from

$$\Delta n_r(r) = -\frac{n_0^3}{2}\left[B_\perp\left(\sigma_\varphi(r)+\sigma_z(r)\right)+B_\parallel\sigma_r(r)\right] \tag{28}$$

$$\Delta n_\varphi(r) = -\frac{n_0^3}{2}\left[B_\parallel\sigma_\varphi+B_\perp\left(\sigma_r(r)+\sigma_z(r)\right)\right] \tag{29}$$

where the quantities $B_\parallel$ and $B_\perp$ are parallel and perpendicular stress-optic coefficient [10].

4. Temperature-dependent change of refractive index

The change of refractive index can be separated into temperature and stress dependent. We discussed the stress-dependent change of refractive index in the previous

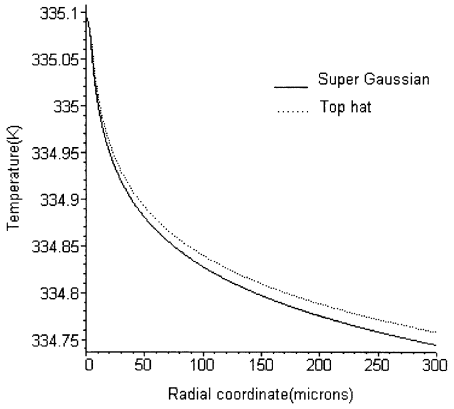

Figure 1. Temperature distribution in the fiber as a function of radial coordinate for a 50 μm beam spot size super-Gaussian profile of order 4 and top hat profile with 180 W pump power at 915 μm.

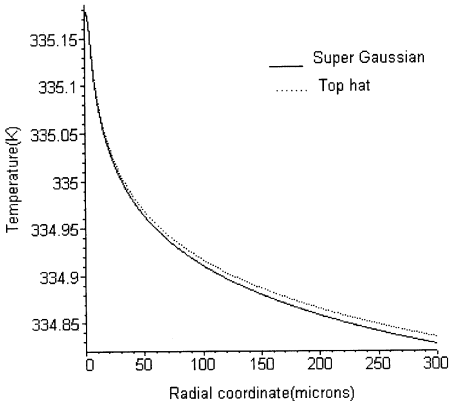

Figure 2. Temperature distribution in the fiber as a function of radial coordinate for a 80 μm beam spot size super-Gaussian profile of order 4 and top hat profile with 180 W pump power at 915 μm.

section. The temperature-dependent change of refractive index can be calculated from the following relation [11]:

$$\Delta n_{\mathrm{T}}(r) = \frac{\mathrm{d}n}{\mathrm{d}T}\left[T(r) - T_{\mathrm{c}}\right], \tag{30}$$

where $\mathrm{d}n/\mathrm{d}T$ depends on the characteristics of the core material.

5. Discussion

Based on the theoretical results obtained in the previous sections, we consider a Yb:glass fiber with a diameter of 9.6 μm and 1.5% doping level [10]. The core region is surrounded by a circular inner cladding region of 330 μm diameter which is also covered by a polymeric outer cladding region of 600 μm diameter. The fiber length is assumed to be 50 m. The pump and lasing wavelengths are 0.915 μm and 1.120 μm respectively. The quantum efficiency of 95% was set and we ignore any non-radiative processes.

Figure 1 shows the fiber temperature distribution in the core and cladding regions as a function of radial coordinate for both the super-Gaussian of order 4 and top hat [10] profile based on eqs (18), (19), and (21). For plotting figure 1, we consider 50 μm beam spot size for super-Gaussian pump beam. In both cases the total power is considered as 180 W. The fiber is cooled by air and its convective heat transfer coefficient was assumed to be 1×10^{-3} W/(cm^2-K). The ambient air temperature T_{c} was assumed to be 300 K and the thermal conductivity was taken as 1.38×10^{-2} W/(cm-K). A temperature difference is seen between the above two kinds of pumping profile especially in the cladding region. According to figure 2, as the spot size (ω_0) increases, such difference will be smaller and so the top hat and the

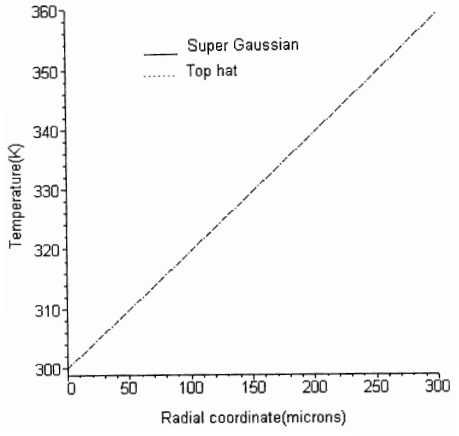

Figure 3. Center temperature in a fiber as a function of radial coordinate for 180 W of 0.915 μm of a super-Gaussian profile pump source of order 4 with 80 μm spot size and a top hat profile pump source.

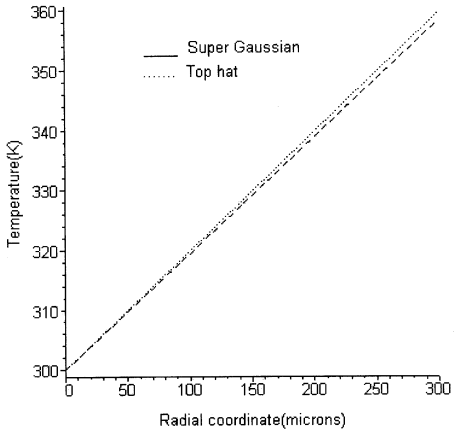

Figure 4. Surface temperature of fiber as a function of radial coordinate for 180 W of 0.915 μm of a super-Gaussian profile pump source of order 4 with 80 μm spot size and a top hat profile pump source.

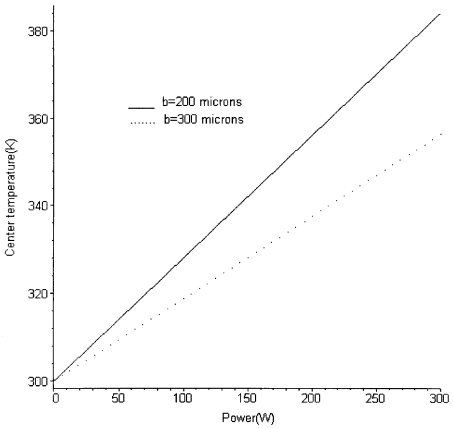

Figure 5. Center temperature in a fiber as a function of radial coordinate for 180 W of a super-Gaussian pump with a core diameter of 9.6 μm and cladding radii of 200 and 300 μm.

super-Gaussian profile will be the same as the beam spot size increases to pump radius size ratio which occur in the high power fiber lasers.

Figure 3 shows the temperature of the center of the fiber for top hat and the super-Gaussian profile pump source. There is no difference in the two models of pumping but the surface temperature as plotted in figure 4 shows a temperature difference if we consider top hat or super-Gaussian profile.

Figure 5 shows the fiber center temperature as a function of pump power from 0 to 300 W for two values of the outer fiber radii of 200 and 300 μm. According

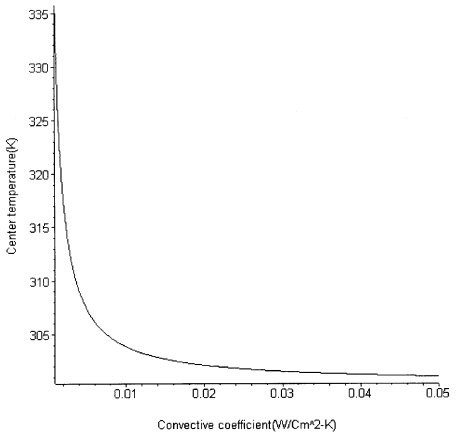

Figure 6. Center temperature of the core as a function of convective coefficient h, for 180 W super-Gaussian pump source with 100 μm spot size.

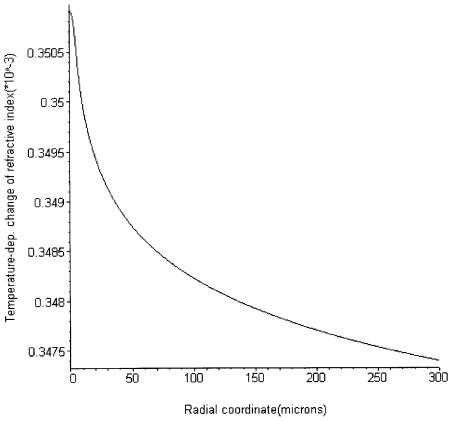

Figure 7. Temperature-dependent change of refractive index as a function of radial coordinate for 180 W of super-Gaussian pump source with 100 μm spot size, and convective coefficient of 1.0×10^{-3} W/(cm^2-K).

to the above results there is no difference between two kinds of pumping. Other parameters are the same as mentioned earlier. This figure clearly suggests that for high power fiber lasers a rather force implementation for cooling is necessary, that is, a force cooling of about 10 times of ordinary air cooling is needed for handling these lasers. This is clearly shown in figure 6.

Figure 7 shows the temperature-dependent change of refractive index vs. the radial coordinate. The pump power is 180 W and the outer fiber radius is 300 μm. We used the value of $(\mathrm{d}n/\mathrm{d}T) = 10^{-5}$ K^{-1} [10]. These refractive index changes can cause some effects such as phase front distortion [13] and thermal beam distortion [14]. Moreover, thermal lens formation which can alter the cavity mode profile and diffraction losses [15] are also important.

Figure 8 shows the three principal stress components σ_r, σ_φ and σ_z as a function of the radial coordinate r for 180 W pump power and 600 μm outer diameter. The heat transfer coefficient and the thermal conductivity are 1.0×10^{-3} W/(cm^2-K) and 1.38×10^{-2} W/(cm-K) respectively. Values of E and ν are 73 Gpa and 0.16 respectively [16].

Thermal expansion coefficient α_{T} was assumed to be 0.51×10^{-6} K^{-1} [16].

As shown in figure 8 in the core region all the stress components are compressive while in the cladding region the stress components are partly compressive and tensile and $r$component of stress is zero at the surface of the cladding.

In figure 9 we plotted radial and tangential components of stress-induced change of refractive index. We used the values $n_0 = 1.45$, 4.5×10^{-8} cm^2/kg and 27.7×10^{-8} cm^2/kg for the value of parallel and perpendicular stress-optic coefficient respectively [16]. This kind of refractive index changes can cause a thermally-induced birefringence in the laser cavity. This effect is due to difference between Δn_r and Δn_φ [11,17].

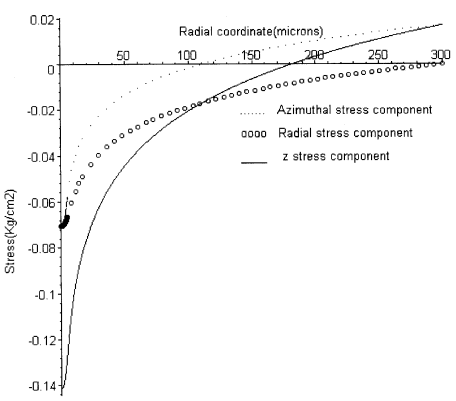

Figure 8. Three stress components as a function of radial coordinate for 180 W of super-Gaussian pump source with 100 μm spot size and convective coefficient of 1.0×10^{-3} W/(cm^2-K).

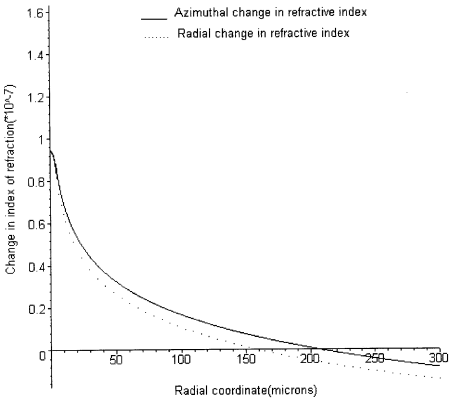

Figure 9. Radial and tangential components of stress-induced change of refractive index as a function of radial coordinate or 180 W of super-Gaussian pump source with 100 μm spot size and convective coefficient of 1.0×10^{-3} W/(cm^2-K).

6. Conclusion

In this paper we presented an analytical treatment of thermo-optics properties of a double-clad Yb:glass fiber laser pumped by a fourth-order super-Gaussian shape diode laser. We obtained temperature distribution in the fiber and then the thermal properties such as temperature-dependent change of refractive index, induced stress and its accompanying change of refractive index are discussed completely. The main feature of this work is to compare a more realistic pump source which is super-Gaussian with the simple sources which have already been analyzed in the literature. It is shown that as the ratio of beam spot size to doped active region size increases, these is no considerable difference in top hat and super-Gaussian profile but when the doped active region radius increases (bulk laser) there is considerable difference between the two pumping profiles. In this regard, one can safely use a non-uniform and multi-mode pump source whose theoretical background and derivations are in hand and be given in this article. We considered the thermal properties such as thermal conductivity and thermal expansion coefficient as constants. The result presented here can be extended for more complicated models [18] in which laser active medium parameter changes are more profound.

References

[1] D L DiGiovanni and M H Muendel, *Opt. Photon. News*, Jan. (1999) 26–30
[2] B Rossi, *Laser Focus World*, May (1997) 143–149
[3] D Richardson, H Offerhaus, J Nilson and A Grudinin, *Laser Focus World*, June (1999) 92–94
[4] B Desthieux, R I Laming and D N Payne, *Appl. Phys. Lett.* **63**, 586 (1993)

[5] R M Percival, D Szebesta, J R Williams, R D T Lauder, A C Tropper and D C Hanna, *Electron. Lett.* **30**, 1598 (1994)
[6] H Takara, A Takada and M Saruwatari, *IEEE Photon. Tech. Lett.* **4**, 241 (1992)
[7] G Nykolas, S A Kramer, J R Simpson, D J DiGiovanni, C R Giles and H M Presby, *IEEE Photon. Tech. Lett.* **3**, 1079 (1991)
[8] W H Cheng and J H Bechtel, *Electron. Lett.* **29**, 2055 (1993)
[9] M H Muendel, in *Proc. SPIE Conf. High-Power Lasers* **3264**, 21 (1999)
[10] David C Brown and Hanna J Hoffman, *IEEE J. Quantum Electron.* **37**, 207 (2001)
[11] W Koechner, *Solid state laser engineering*, 5th ed (Springer, 1999) p. 408
[12] M Abramawitz and I A Stegun (eds), *Handbook of mathamatical function* (Dover, New York, 1965) p. 227
[13] A Giesen, H Hugel, A Voss, K Witting, U Brauch and H Opower, *Appl. Phys.* **B58**, 365 (1994)
[14] C Pfistener, R Weber, H P Weber, S Merazzi and R Gruber, *IEEE J. Quantum Electron.* **30**, 1605 (1994)
[15] Justin L Blows, G W Forbes and Gudidth M Dawes, *Opt. Commun.* **186**, 111 (2000)
[16] M Bass, Handbook of optics, in: *Measurements and property* (sponsored by the optical society of Amirica) (McGraw-Hill, New York, 1995)
[17] M Schmid, R Weber, Tomas Graf, M Roos and Heinz P Weber, *IEEE J. Quantum Electron.* **36**, 620 (2000)
[18] W F Krupke, M D Shinn, J E Marion, J A Carid and S E Stokowski, *J. Opt. Soc. Am.* **3**, 102 (1986)